CONDENSED MATTER PHYSICS

Three-dimensional magnetism and the Dzyaloshinskii-Moriya interaction in $S = 3/2$ kagome staircase $Co_3V_2O_8$

Joel S. Helton[1,2]*, Nicholas P. Butch[2], Daniel M. Pajerowski[2†], Sergei N. Barilo[3], Jeffrey W. Lynn[2]

Time-of-flight neutron data reveal spin waves in the ferromagnetic ground state of the kagome staircase material $Co_3V_2O_8$. While previous work has treated this material as quasi–two-dimensional, we find that an inherently three-dimensional description is needed to describe the spin wave spectrum throughout reciprocal space. Moreover, spin wave branches show gaps that point to an unexpectedly large Dzyaloshinskii-Moriya interaction on the nearest-neighbor bond, with $D_1 \geq J_1/2$. A better understanding of the Dzyaloshinskii-Moriya interaction in this material should shed light on the multiferroicity of the related $Ni_3V_2O_8$. At a higher temperature where $Co_3V_2O_8$ displays an antiferromagnetic spin density wave structure, there are no well-defined spin wave excitations, with most of the spectral weight observed in broad diffuse scattering centered at the (0, 0.5, 0) antiferromagnetic Bragg peak.

INTRODUCTION

Frustrated quantum spin systems—where no collinear magnetic order can simultaneously satisfy all interactions in the spin Hamiltonian due to the geometry of the lattice, disorder, or competing interactions—will often feature highly degenerate ground-state manifolds with unusual spin correlations and excitations (*1*). Subtle perturbations can lead to very different physics in similar systems by selecting between nearly degenerate possible ground states. Multiferroic materials, with coexisting magnetic and electric order parameters (*2*), offer technological promise but are relatively rare in part because ferroelectric order requires a noncentrosymmetric space group that breaks inversion symmetry while magnetic order instead breaks time reversal symmetry.

A class of compounds $M_3V_2O_8$, where M is a divalent cation such as Mn, Co, Ni, Cu, or Zn (*3*–*8*), form the kagome staircase lattice structure with M^{2+} ions residing on buckled planes of corner-sharing triangles. $Co_3V_2O_8$ (CVO) features $S = 3/2$ Co^{2+} ions arranged on this lattice. As the structure consists of edge-sharing CoO_6 octahedra, the Co—O—Co bond angles are quite close to 90° for the bonds between adjacent Co ions; the resulting weak nearest-neighbor superexchange interactions yield the opportunity for other interactions to play a significant role in selecting the ordered state and driving the spin dynamics. Previous single-crystal (*9*) neutron diffraction experiments have revealed a rich variety of magnetic phases. The ground state of CVO is ferromagnetic with all spins aligned along the crystallographic a axis. Above $T_C = 6.2$ K, CVO enters a phase featuring a transversely polarized antiferromagnetic spin density wave (SDW) state with a propagation vector of $\vec{k} = (0, \delta, 0)$ that is perpendicular to the buckled kagome planes. The propagation vector evolves with temperature, featuring commensurate lock-in phases at $\delta = 0.33$ and $\delta = 0.5$ interspersed with two distinct incommensurate SDW phases that yield to a paramagnetic phase above $T_N = 11.3$ K. Magnetic phase diagrams for CVO with an applied magnetic field (*10*–*13*) reveal a complex evolution of the magnetic phases and a new commensurate lock-in of the SDW at $\delta = 0.4$. The phonon thermal conductivity in CVO is significantly suppressed at temperatures slightly above T_C due to scattering of phonons by critical spin fluctuations (*14*); the nearly 100-fold increase in thermal conductivity under the application of a magnetic field suggests the possible use of CVO as a heat switch.

$Ni_3V_2O_8$ (NVO) features $S = 1$ Ni^{2+} ions arranged on a nearly identical kagome staircase structure, with competing interactions that also yield a complex magnetic phase diagram (*6*). The low-temperature incommensurate phase in this material is magnetically ordered into an inversion symmetry breaking helical order (*15*, *16*) that appears simultaneously with ferroelectric polarization (*17*) and multiferroic domains that can be controlled by an applied electric field (*18*, *19*). While CVO is not ferroelectric, the same vibrational mode that leads to polarization in NVO is highly sensitive to an applied magnetic field (*20*), and there is evidence of a field-induced structural distortion (*21*). Because the Dzyaloshinskii-Moriya (DM) interaction likely plays a role in stabilizing the helical order of the ferroelectric phase in NVO, a complete understanding of the spin Hamiltonian including DM terms in structurally similar CVO should further the understanding of the multiferroic behavior in NVO.

RESULTS

CVO has an orthorhombic unit cell with $a = 6.0262(6)$ Å, $b = 11.4812(6)$ Å, and $c = 8.29760(9)$ Å and space group *Cmca* (#64). There are two crystallographically distinct Co sites: Co1 ions occupy the 4*a* Wyckoff positions at (0, 0, 0), while the Co2 ions occupy the 8*e* Wyckoff positions at (0.25, y, 0.25), with $y = 0.1304(6)$. As shown in Fig. 1A the Co ions form buckled kagome lattice planes of corner-sharing triangles. The Co2 sites form chains running along the a axis that are connected by the Co1 sites; because of this, the Co1 ions are often referred to as the cross-ties, while the Co2 chains are called the spines. Each buckled kagome plane features a central plane of Co1 cross-tie sites that connect to Co2 spines that alternate above and below the cross-tie plane along the b axis.

We consider a spin Hamiltonian consisting of Heisenberg interactions J, DM interactions $\vec{D}$, and single-ion anisotropies A

[1]Department of Physics, United States Naval Academy, Annapolis, MD 21402, USA. [2]NIST Center for Neutron Research, National Institute of Standards and Technology, Gaithersburg, MD 20899, USA. [3]Institute of Solid State and Semiconductor Physics, Academy of Sciences, Minsk 220072, Belarus.
*Corresponding author. Email: helton@usna.edu
†Present address: Neutron Scattering Division, Oak Ridge National Laboratory, Oak Ridge, TN 37831, USA.

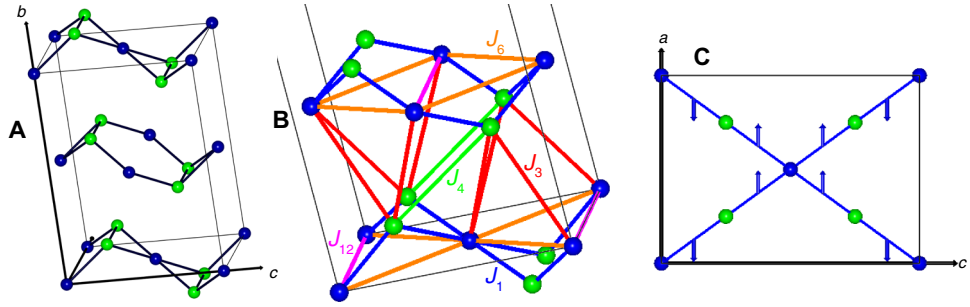

Fig. 1. Crystal structure. (**A**) Crystal structure of CVO. Co1 cross-tie sites are shown in blue, and Co2 spine sites are shown in green. (**B**) Relevant Heisenberg exchange couplings. (**C**) The arrow at the midpoint of each nearest-neighbor bond shows the direction of the DM component $D_{1,x}$ using the convention that the cross-product of the spins is defined with the spine site first. This component is positive for bonds connecting a cross-tie site at $z = c/2$ and negative for bonds connecting a cross-tie site at $z = 0$.

$$\mathcal{H} = \sum_{\langle i,j \rangle} J_{\mathrm{ij}} \vec{S}_i \cdot \vec{S}_j + \vec{D}_{\mathrm{ij}} \cdot (\vec{S}_i \times \vec{S}_j) + \sum_{i,\mu} A_{i,\mu} S^2_{i,\mu} \qquad (1)$$

where, in the summation, i and j represent individual spins and $\mu = x$, y, or z. The Heisenberg interactions considered are shown in Fig. 1B. The first nearest-neighbor interaction, J_1, acts over a distance of 2.97 Å between a cross-tie and spine site [this interaction has been previously termed J_{sc} for this reason (*9*, *22*)]. The second nearest-neighbor distance is 3.01 Å between adjacent spine sites; previous spin wave measurements were consistent with this interaction being zero (*22*). The third nearest-neighbor interaction, J_3, acts over a distance of 4.96 Å between the spine sites of one buckled kagome plane and the cross-tie sites on an adjacent plane. The fourth nearest-neighbor interaction, J_4, acts over a distance of 4.98 Å between spine sites on adjacent buckled kagome planes. Weak antiferromagnetic 6th and 12th nearest-neighbor interactions are also included in our model. The sixth nearest-neighbor interaction, J_6, acts over a distance of 5.13 Å between the nearest cross-tie sites within a single plane. The 12th nearest-neighbor interaction, J_{12}, acts over a distance of 6.03 Å between two cross-tie spins separated by one lattice vector $\vec{a}$.

We also consider a DM interaction on the nearest-neighbor bond. There is no mirror plane containing the midpoint of this bond so all three components of $\vec{D}_1$ are allowed by symmetry. We find that only the component along the a axis, $D_{1,x}$, affects the spin wave dispersion. If we define the order of the cross-product as $\vec{D}_1 \cdot (\vec{S}_{\mathrm{s}} \times \vec{S}_{\mathrm{c}})$ with the spine site first and the cross-tie site second, then $D_{1,x}$ is positive for all nearest-neighbor bonds connecting a cross-tie site at $z = c/2$, and $D_{1,x}$ is negative for all nearest-neighbor bonds connecting a cross-tie site at $z = 0$. This definition is shown in Fig. 1C.

The spin wave spectra of CVO in the ferromagnetic phase were measured using the Disk Chopper Spectrometer (DCS) time-of-flight instrument at the National Institute of Standards and Technology (NIST) Center for Neutron Research in both the (H K 0) and (0 K L) scattering planes. These sample geometries provide data along all three principal axes in reciprocal space and directions perpendicular to the buckled kagome planes. Fits of the measured spin wave dispersion to a model Hamilton and simulations of the neutron spin wave spectra were performed using the SpinW software (*23*). The spin values were fixed to $S = 3/2$, and the ground state was set to all spins aligned along the a axis. The magnetization hard axis is along the crystallographic b axis (*7*), so the anisotropy parameters along the b axis were set to zero ($A_{i,y} = 0$) and anisotropy parameters along the other two directions are expected to be negative. The ferromagnetic ground state at 3.1 K features ordered moments of 1.54 and 2.73 μ_{B} (bohr magneton) on the cross-tie and spine sites, respectively (*9*). The reduced moment on the cross-tie sites has been modeled by lowering the magnetic form factor for this site by a factor of 0.75, so that the form factor squared is proportional to the ordered moment. The missing magnetic moment from the Co cross-tie sites is found on the O and V sites when an applied field polarizes the sample (*24*). This suggests that the cobalt spin value could be reduced from $S = 3/2$, although an enhanced Curie constant in the high-temperature susceptibility (*7*) suggests otherwise. The fits were repeated using reduced Co spin values, which results in larger fit values for the Hamiltonian parameters and a comparable quality fit; these results are presented in the Supplementary Materials.

The best fit to the measured spin wave dispersion resulted in the parameters listed in Table 1; unless specified otherwise, the spin wave simulations use these parameters. This set of fitting parameters replicates the energy positions of the measured spin wave excitations in the lower energy branch (roughly between 1.5 and 2.5 meV) quite well throughout the (H K 0) and (0 K L) scattering planes, as discussed and further demonstrated in the Supplementary Materials. Figure 2 shows data and simulations for spin waves along the [0 K 0] and [1 K 0] directions, while Fig. 3 shows data and simulations for spin waves along the [H 1 0] and [H 1.35 0]. Further, this proposed Hamiltonian also replicates the measured spectra of the lower energy branch in previously reported data in the (H 0 L) scattering plane (*22*, *25*) and along the [0 K K/4 + 2.5] direction (*26*). There is, however, some discrepancy between the measured and simulated dispersion for the higher energy branch (roughly between 4 and 6 meV) particularly along the [0 0 L] direction. Further interactions might need to be included to fully model the higher energy branch along this direction. The antiferromagnetic SDW state displayed by CVO at slightly higher temperatures likely indicates the presence of at least one antiferromagnetic interaction between spins on adjacent kagome planes; however, these spin wave data indicate that the between-plane antiferromagnetic interactions must be fairly weak.

The excitation spectra were also measured at $T = 9.2$ K, where CVO displays an antiferromagnetic SDW magnetic structure with a commensurate propagation vector of $\vec{k} = (0, 0.5, 0)$ (*9*). These data are shown in Fig. 4. Well-defined spin waves are not observed; instead, the spectral weight is dominated by broad quasi-elastic scattering near antiferromagnetic Bragg peaks.

DISCUSSION

Previous work on CVO has described the material as quasi–two-dimensional (2D) (*27*, *25*), where the dominant magnetic interactions were entirely within the buckled kagome planes. The spin wave

Table 1. Hamiltonian parameters. Spin Hamiltonian parameters for the displayed simulations. All parameters are given in units of millielectron volts. *J* values < 0 are ferromagnetic, while *J* values > 0 are antiferromagnetic.

J_1	−0.21 ± 0.02	$A_{c,x}$	−0.60 ± 0.03
J_3	−0.14 ± 0.02	$A_{c,z}$	−0.72 ± 0.03
J_4	−0.12 ± 0.03	$A_{s,x}$	−1.22 ± 0.03
J_6	0.010 ± 0.006	$A_{s,z}$	−0.37 ± 0.04
J_{12}	0.035 ± 0.005	$D_{1,x}$	0.12 ± 0.03

dispersion along the [*H* 0 0] and [0 0 *L*] directions has been measured (*22*), and two spin wave branches were observed, with the higher energy branch significantly weaker in intensity and broader in energy. These data were well fit to a model with only ferromagnetic nearest-neighbor interactions (J_1) and single ion anisotropy terms for both the cross-tie and spine sites. However, with the additional data we have collected, we find that a description of the spin wave spectra throughout momentum space requires a fully 3D spin Hamiltonian. A quasi-2D spin Hamiltonian with only first nearest-neighbor interactions would feature dispersionless spin waves along the [0 *K* 0] direction. The measured spin wave spectrum along the [0 *K* 0] direction, as shown in Fig. 2B, is quite dispersive with a bandwidth (about 1 meV) comparable to that observed in scans along the [*H* 0 0] or [0 0 *L*] directions. This demonstrates that there are interactions between kagome planes comparable in strength to the in-plane J_1.

The best fit to the spin wave dispersion data suggested ferromagnetic first, third, and fourth nearest-neighbor interactions with $J_1 = -0.21 \pm 0.02$ meV, $J_3 = -0.14 \pm 0.02$ meV, and $J_4 = -0.12 \pm 0.03$ meV. While other interactions are considered to fully describe the spin wave dispersion, these three interactions are sufficient to generally describe the spin wave bandwidth for most of the measured data. The second nearest-neighbor interaction, between adjacent spine sites, was also considered but is not included in these simulations. When included in the fit, the J_2 interaction refined to a very small magnitude and did not substantially affect any simulated results. A Hamiltonian dominated by ferromagnetic interactions is unusual, given that CVO displays an antiferromagnetic SDW state at temperatures between 6.2 and 11.3 K. The magnetic structure of this SDW state at temperatures yielding a δ = 0.5 lock-in has been deduced from powder neutron diffraction (*9*). While that structure is antiferromagnetic, it does not contain any pair of antiferromagnetically aligned spins connected by one of these three interactions; all spins connected by J_4 are ferromagnetically aligned, while all spins connected by J_1 or J_3 are either ferromagnetically aligned or feature a cross-tie spin with no ordered moment. This suggests that antiferromagnetic interactions between kagome planes that are too weak to be determined from spin wave data select the antiferromagnetic SDW structures. The Curie-Weiss temperature for CVO with only these three ferromagnetic interactions would be given by $\theta_{CW} = -\frac{S(S+1)}{3k_B}\left(\frac{8}{3}J_1 + \frac{8}{3}J_3 + \frac{4}{3}J_4\right) \approx 16$ K. This value is considerably larger than the transition temperature; including at least one additional antiferromagnetic interaction between kagome planes would lower the magnitude of the predicted Curie-Weiss temperature, although this difference could also indicate the effects of frustration.

The fit values for the anisotropy parameters were $A_{c,x} = -0.60 \pm 0.03$ meV and $A_{c,z} = -0.72 \pm 0.03$ meV for the cross-tie sites and $A_{s,x} = -1.22 \pm 0.03$ meV and $A_{s,z} = -0.37 \pm 0.04$ meV for the spine sites. These fit parameters are all negative, so the *b* axis is the hard axis for both sites. When averaged over the two sites, the *a* axis is the easy axis in agreement with magnetization measurements (*7*), although the *c* axis is slightly easier than the *a* axis for the cross-tie sites. The cross-tie sites have been proposed to order along the *c* axis when a 15-T magnetic field is applied along the *b* axis, effectively decoupling the spine and cross-tie sites; it is the spine sites that have the strongest easy-axis anisotropy along the *a* axis although the spine sites will polarize along the *b* axis in this scenario but not the cross-ties (*25*).

Single-ion anisotropy and several symmetric Heisenberg exchange terms are sufficient to generally describe the bandwidth of the measured spin waves. However, the measured spin wave energies at many positions in momentum space are split away from the rest of the smoothly dispersing branch by about 0.3 meV. This is shown in Fig. 2B for the [0 *K* 0] direction and Fig. 2E for the [1 *K* 0] direction. This splitting can be explained by the introduction of a DM interaction along the nearest-neighbor bond with a component along the *a* axis of $D_{1,x} = 0.12 \pm 0.03$ meV. Figure 2 (A and D) shows simulations with no DM interaction but with all other parameters the same as in Table 1. These simulations show no splitting at the relevant positions. The simulations with the DM term included, shown in Fig. 2 (C and F), provide a much better fit to the data. The white dashed lines in the simulations in Fig. 2 represent the dispersion of two particular spin wave modes. The simulations with no DM term each feature a smooth sinusoidally dispersing mode and a flat mode; the dispersing mode has a large intensity along [0 *K* 0], while along [1 *K* 0], it is the flat mode that features a large intensity. The inclusion of a DM interaction causes an avoided crossing between the two modes, yielding the observed splitting as the spin wave intensity shifts between the two modes near the avoided crossing.

All three components of the DM vector are allowed by symmetry, but inclusion of the other two components did not affect the simulated spin wave spectra. A DM interaction on a bond arising from superexchange is expected to lie perpendicular to the plane containing the two spins and the mediating anion (*28*). In CVO, this would suggest that there is little component along the *c* axis ($D_{1,z} \approx 0$) but that the component along the *b* axis should be comparable in magnitude to the component along the *a* axis, meaning that the magnitude of the DM vector could be as large as $D_1 \approx 0.17$ meV or $D_1 \approx 0.8\, J_1$.

The DM interaction on the kagome lattice has been a topic of interest for years (*29*), although it is typically assumed that $D \ll J$. The large DM term found in CVO, with $D_{1,x} \approx 0.6\, J_1$, is notable in comparison. Recently, however, materials with very large DM terms have exhibited unique physics. For example, topological excitations including skyrmions have been predicted for kagome lattice ferromagnets with $D \approx 0.4J$ (*30*), and the $S = 1/2$ helical-honeycomb antiferromagnet α-$Cu_2V_2O_7$ with $D \approx J$ displays nonreciprocal spin waves (*31*). The pyrochlore ferromagnet $Lu_2V_2O_7$ with $D \approx J/3$ exhibits the magnon Hall effect (*32*), although it has been argued that, in this material, the apparently large DM interaction is actually caused by other terms in the Hamiltonian (*33*).

The DM interaction as a possible microscopic mechanism supporting the existence of multiferroicity has long been appreciated (*34*–*36*) because this interaction can lead to helical magnetic order that breaks inversion symmetry. A DM interaction term likely plays a role in stabilizing the magnetic order in the ferroelectric phase of NVO; DM terms on the bonds connecting two spine sites and also the bond connecting a spine with a cross-tie have been considered

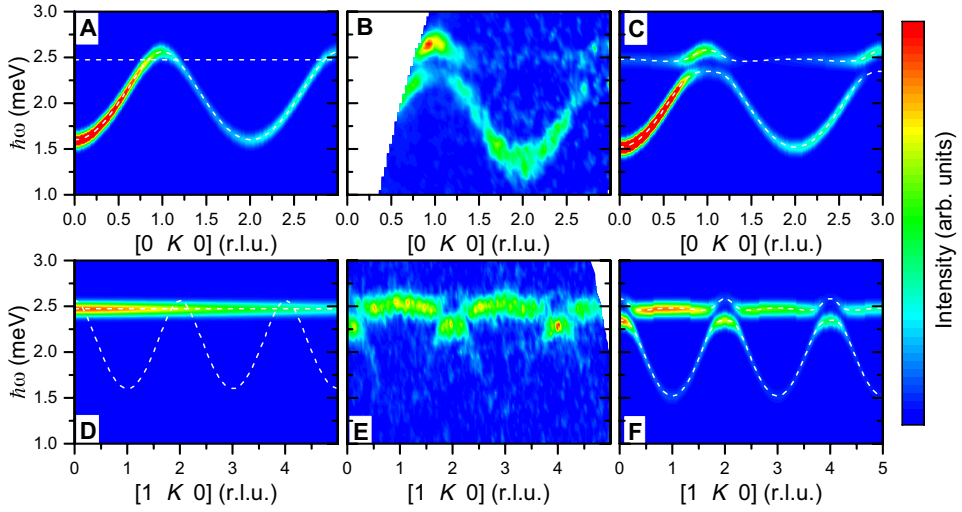

Fig. 2. Spin wave data and simulations with the DM interaction. (**A**) Simulation of spin waves along [0 *K* 0] without any DM term, showing a smooth dispersion. The white dashed lines represent the dispersion of two spin wave modes. (**B**) Measured spin wave data along [0 *K* 0] at 2.8 K. The data are integrated over $-0.05 \leq H \leq 0.05$. The dispersion is distinctively not smooth, with the spin wave energy at (0, 1, 0) split away from the rest of dispersion by about 0.3 meV. (**C**) Simulation of spin waves along [0 *K* 0] with a DM term of $D_{1,x} = 0.12$ meV. An avoided crossing between the two modes produces the observed spitting. (**D**) Simulation of spin waves along [1 *K* 0] without any DM term, showing a smooth flat band. (**E**) Measured spin wave data along [1 *K* 0] at 2.8 K. The data are integrated over $0.95 \leq H \leq 1.05$. The spin wave energy near $K = 0$, 2, and 4 is split lower than the rest of the dispersion by about 0.3 meV. (**F**) Simulation of spin waves along [1 *K* 0] with a DM term of $D_{1,x} = 0.12$ meV. The simulation including the DM term provides a good fit to the data. arb. units, arbitrary units.

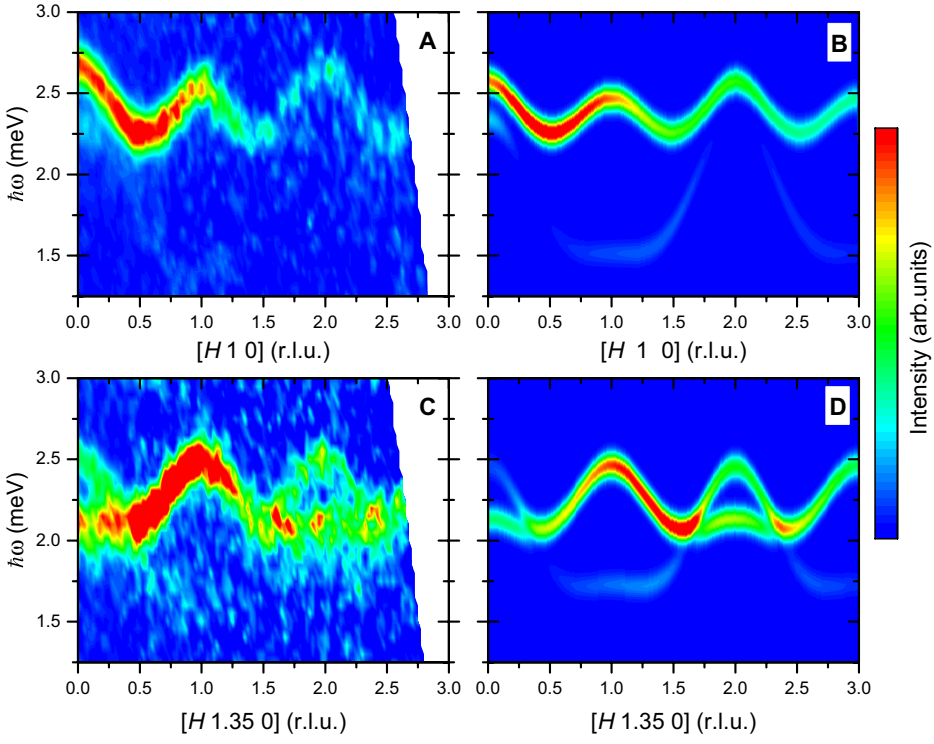

Fig. 3. Spin wave data and simulations with J_{12}. (**A**) Measured spin wave data along [*H* 1 0] at 2.8 K. The data are integrated over $0.95 \leq K \leq 1.05$. (**B**) Simulation of spin waves along [*H* 1 0]. The simulation captures the asymmetry of the dispersion, with the energy slightly higher at $H = 0$ than at $H = 1$. (**C**) Measured spin wave data along [*H* 1.35 0] at 2.8 K. The data are integrated over $1.3 \leq K \leq 1.4$. (**D**) Simulation of spin waves along [*H* 1.35 0]. The simulation captures the observed splitting at (2, 1.35, 0).

(*15*), and it has been suggested that the DM interaction between two spine sites must have a component along the *a* axis, which would require a magnetoelastic distortion in this phase to break mirror plane symmetry (*18*). The spin wave results on CVO show that the DM interaction can be quite significant on the superexchange bonds of this structure. The ferroelectric phase of NVO remains stable over an expanded temperature range under moderate doping of Co for Ni (*37*, *38*); an increased DM interaction on bonds connected to a Co ion doped into the system could be one reason for the relative stability of the helical magnetic structure under doping.

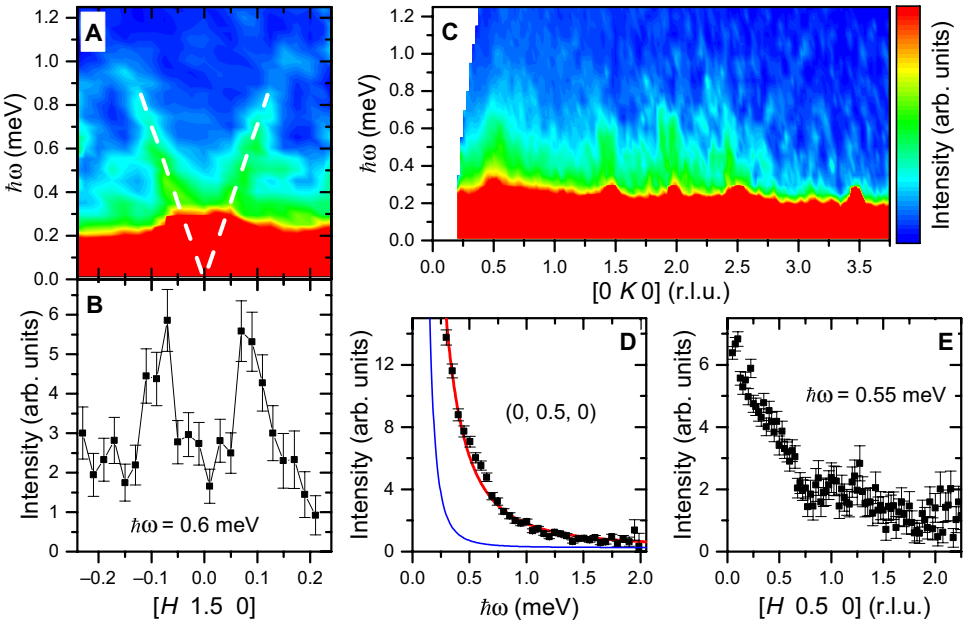

Fig. 4. Spin excitation data at $T = 9.2$ K. (**A**) Dispersive excitations emanating from the antiferromagnetic Bragg peak at (0,1.5,0). The data are integrated over $1.45 \leq K \leq 1.55$. The dashed lines are guides to the eye, representing a dispersion with a slope of 6.8 meV · Å. (**B**) The data are integrated over $1.45 \leq K \leq 1.55$ and 0.4 meV $\leq \hbar\omega \leq$ 0.8 meV. (**C**) The spin excitation spectrum along [0 *K* 0]. The data are integrated over $-0.1 \leq H \leq 0.1$. (**D**) Energy spectrum at $\vec{Q} =$ (0,0.5,0). The data are integrated over $-0.1 \leq H \leq 0.1$ and $0.4 \leq K \leq 0.6$. The red line is a fit to a Lorentzian function with a half width at half maximum (HWHM) of 0.37 meV. The blue line is an estimate of the elastic scattering from the Bragg peak convolved with the energy resolution. (**E**) Spin excitations along [*H* 0.5 0]. The data are integrated over $0.4 \leq K \leq 0.6$ and 0.3 meV $\leq \hbar\omega \leq$ 0.8 meV.

The simulated spin wave spectra presented here include a very weak antiferromagnetic sixth nearest-neighbor interaction, $J_6 = 0.010 \pm 0.006$ meV, between cross-tie sites in the same plane. The energy level of the flat spin wave modes in simulations without any DM term, such as in Fig. 2 (A and D), is very sensitive to this term in the Hamiltonian. A value of $J_6 = 0.01$ meV was chosen to lower this flat mode by a small amount so as to best match the observed data once the DM term was included. A previous work (*25*) had also suggested an antiferromagnetic J_6 because of an antiferromagnetic ordering pattern observed on the cross-tie sites with a 15-T magnetic field applied along the *b* axis. Given the symmetry relations of the DM interaction on the nearest-neighbor bond, shown in Fig. 1C, a nonzero $D_{1,x}$ would also energetically favor this magnetic structure where spine sites are ferromagnetically ordered along the *b* axis and cross-ties are antiferromagnetically ordered along the *c* axis.

The Hamiltonian described so far provides a good description of the lower energy spin wave mode throughout almost all of the measured positions in momentum space; however, this description notably fails to model the spin wave dispersion along the [*H* 1 0] direction. The observed spin wave dispersion along this direction, as shown in Fig. 3A, is dispersive with a bandwidth of about 0.5 meV. While close to sinusoidal, this dispersion is slightly asymmetric with the spin wave located at 2.663 ± 0.004 meV at the (0, 1, 0) position and only 2.544 ± 0.007 meV at the (1, 1, 0) position. A simulation with only the Hamiltonian terms described so far would be almost flat along this direction. Allowing for a weak antiferromagnetic 12th nearest-neighbor interaction captures this dispersion, including the slight asymmetry, almost perfectly as shown in Fig. 3B. It is unusual that interactions out to the 12th nearest neighbor would be relevant; however, the dispersion along this direction is quite sensitive to this interaction, and the fit value of $J_{12} = 0.035 \pm 0.005$ meV is quite small.

In addition to Heisenberg exchange interactions presented in Table 1, the remaining interactions up through 11th nearest neighbor were considered, as was J_{lu} (*9*), covering the 9.66-Å distance between a lower spine site of one kagome plane and an upper spine site on the higher kagome plane. Including these terms did not appreciably improve the fit and led to fairly small refined values (less than 0.05 meV in magnitude). It should be noted that the fit values for J_6 and J_{12} are smaller than 0.05 meV, but the spin wave spectra are sufficiently sensitive to those parameters that their inclusion does improve the fit while including other farther-distance terms does not.

Once this value of J_{12} is included, the spin wave spectra are well modeled even at positions where the DM interaction causes a significant splitting. Figure 3C shows the measured spin wave spectrum along the [*H* 1.35 0] direction; this direction was chosen to maximize the effect of both J_{12} and $D_{1,x}$ on the simulated spectrum. The spin wave spectrum is well described by the simulation shown in Fig. 3D, including the observation of two distinct spin wave modes, at energies of 2.1 and 2.5 meV, at the (0, 1.35, 0) or (2, 1.35, 0) position.

The spin excitation spectrum of CVO at $T = 9.2$ K, in the antiferromagnetic SDW phase, is shown in Fig. 4. Well-defined spin wave excitations were not observed at this temperature; this is not particularly unusual as neutron diffraction measurements (*39*) found that antiferromagnetic Bragg peaks were broader than the instrumental resolution at many temperatures in the SDW regime of CVO and spin waves in the incommensurate phases of NVO (*40*) are very diffuse. The only dispersive-like feature observed at $T = 9.2$ K is shown in Fig. 4A with spin waves weakly emanating from the (0, 1.5, 0) antiferromagnetic Bragg position. Figure 4B shows a cut along the [*H* 1.5 0] direction centered at an energy transfer of 0.6 meV, and peaks are observed at $|H| = 0.085 \pm 0.004$ reciprocal lattice units (r.l.u.), indicating an effective spin wave velocity of about 6.8 meV·Å.

The spin excitation spectrum at $T = 9.2$ K is shown in Fig. 4C along the [0 K 0] direction. A columnar-like excitation can be seen emanating from the positions at $K = 0.5$, 1.5, 2, and 2.5 up to energies around 0.75 meV. The excitation emanating from the (0, 2, 0) position is due to acoustic phonons. This is clear from the fact that this position has no antiferromagnetic Bragg peak and that the excitation is also present at 2.8 K. The excitations emanating from the $K = 0.5$, 1.5, and 2.5 positions are present only in the SDW phase. If these represent dispersive excitations, then the spin wave velocity is too high or the damping is too large to resolve well-defined modes. The scattering near (0, 0.5, 0) is the strongest and by far the broadest in momentum space, indicating significant diffusive scattering at this position.

The energy dependence of the diffuse scattering at (0, 0.5, 0) is shown in Fig. 4D. This quasi-elastic scattering can be fit to a Lorentzian function with a half width at half maximum (HWHM) of 0.37 meV. Figure 4E shows inelastic scattering over an energy range meant to capture most of this spectral weight (0.3 meV $\leq \hbar\omega \leq$ 0.8 meV) along [H 0.5 0]. The first few data points, with $0.05 \leq H \leq 0.10$, are particularly high; this likely represents dispersive scattering comparable to that shown in Fig. 4A but at this position, it is largely obscured by the much stronger diffuse scattering. The diffuse scattering near (0, 0.5, 0) is very broad, with an HWHM of 0.5 Å^{-1} along the [H 0.5 0] direction.

In summary, the spin wave spectrum of CVO in its ferromagnetic ground state has been measured throughout the (H K 0) and (0 K L) scattering planes. The best fit to the data indicates an inherently 3D spin Hamiltonian of ferromagnetic first, third, and fourth nearest-neighbor interactions where the longer distance interactions are about half as strong as the dominant nearest-neighbor exchange between a spine site and a cross-tie site. This stands in contrast to previous analysis of CVO, which had treated the material as quasi-2D. Weak antiferromagnetic couplings J_6 and J_{12} improve the fit, although additional antiferromagnetic interactions might also be present given the antiferromagnetic SDW structure that CVO displays at intermediate temperatures. Most notably, a complete description of the measured spin wave spectra requires a DM interaction along the nearest-neighbor bond with $D \geq J/2$. While the single-ion anisotropy and Heisenberg exchange terms are sufficient to produce a collinear ferromagnetic ground state, the presence of such a significant DM term suggests that CVO might be close to a more exotic ordered state. At $T = 9.2$ K, CVO displays an antiferromagnetic SDW state with a propagation vector of $\vec{k} = (0, 0.5, 0)$. Despite the ordered state, well-defined spin waves are not observed. Instead, the spectrum consists mainly of the diffuse quasi-elastic scattering centered at $\vec{Q} = (0,0.5,0)$ and weak modes dispersing along the [H 1.5 0] direction.

MATERIALS AND METHODS

Large single-crystal samples of CVO were grown by the floating zone technique using an optical image furnace. Neutron spectroscopy measurements were performed using the DCS time-of-flight instrument at the NIST Center for Neutron Research in low-resolution mode. A 4.2-g single-crystal sample was mounted in the (H K 0) scattering plane and cooled to $T = 2.8$ K using a closed-cycle refrigerator. The sample was rotated through 180° in 1° increments with 8 min of counting time per angle. This was performed with incident neutron wavelengths of both 2.5 and 3.7 Å. In an additional experiment using the DCS, a 3.6-g single-crystal sample was mounted in the (0 K L) scattering plane and cooled to $T = 1.6$ K while placed inside a 10-T vertical field superconducting magnet. In zero field, the sample was rotated through two 60° wedges (with $\vec{Q}$ roughly parallel to the b axis and c axis) in 1° increments. Measurements with an incident wavelength of 2.5 Å had 8 min of counting time per angle, while measurements with an incident wavelength of 3.7 Å had 6 min of counting time per angle. For the experiment in the (H K 0) scattering plane, the sample was heated to $T = 9.2$ K, where CVO displays an antiferromagnetic SDW phase with a propagation vector of $\vec{k} = (0,0.5,0)$, and the above measurements were repeated.

The DCS instrument produces a 3D array of intensity data as a function of energy transfer and the two directions of reciprocal space within the scattering plane. This dataset can then be partitioned to produce the dispersion relation throughout reciprocal space. The dispersion relation of spin waves throughout a lower energy branch (roughly between 1.5 and 2.5 meV) was determined by fitting energy cuts to the data measured with an incident wavelength of 3.7 Å. The dispersion relation of spin waves in a higher energy branch (roughly between 4 and 6 meV) was determined by fitting energy cuts to the data measured with an incident wavelength of 2.5 Å. The energy resolution (HWHM) of DCS at the elastic line in low-resolution mode is 0.14 meV for an incident wavelength of 3.7 Å and 0.46 meV for an incident wavelength of 2.5 Å. The dispersion relations obtained from these cuts were fit to the model Hamiltonian using SpinW. The data were folded across $H = 0$ and $K = 0$ to maximize intensity in a single quadrant of reciprocal space for all figures except for Fig. 4 (A and B), which were not folded across $H = 0$ to demonstrate symmetrically dispersing excitations. Error bars and uncertainties on fit parameters throughout this paper are statistical in nature and represent 1 SD.

SUPPLEMENTARY MATERIALS

Supplementary material for this article is available at http://advances.sciencemag.org/cgi/content/full/6/18/eaay9709/DC1

REFERENCES AND NOTES

1. L. Balents, Spin liquids in frustrated magnets. *Nature* **464**, 199–208 (2010).
2. S.-W. Cheong, M. Mostovoy, Multiferroics: A magnetic twist for ferroelectricity. *Nat. Mater.* **6**, 13–20 (2007).
3. N. Rogado, G. Lawes, D. A. Huse, A. P. Ramirez, R. J. Cava, The kagomé-staircase lattice: Magnetic ordering in $Ni_3V_2O_8$ and $Co_3V_2O_8$. *Solid State Commun.* **124**, 229–233 (2002).
4. N. Rogado, M. K. Haas, G. Lawes, D. A. Huse, A. P. Ramirez, R. J. Cava, β-$Cu_3V_2O_8$: Magnetic ordering in a spin-$\frac{1}{2}$ kagomé-staircase lattice. *J. Phys. Condens. Matter* **15**, 907–914 (2003).
5. G. Balakrishnan, O. A. Petrenko, M. R. Lees, D. M. K. Paul, Single crystals of the anisotropic kagomé staircase compounds $Ni_3V_2O_8$ and $Co_3V_2O_8$. *J. Phys. Condens. Matter* **16**, L347–L350 (2004).
6. G. Lawes, M. Kenzelmann, N. Rogado, K. H. Kim, G. A. Jorge, R. J. Cava, A. Aharony, O. Entin-Wohlman, A. B. Harris, T. Yildirim, Q. Z. Huang, S. Park, C. Broholm, A. P. Ramirez, Competing magnetic phases on a "kagomé staircase". *Phys. Rev. Lett.* **93**, 247201 (2004).
7. R. Szymczak, M. Baran, R. Diduszko, J. Fink-Finowicki, M. Gutowska, A. Szewczyk, H. Szymczak, Magnetic field-induced transitions in geometrically frustrated $Co_3V_2O_8$ single crystals. *Phys. Rev. B* **73**, 094425 (2006).
8. E. Morosan, J. Fleitman, T. Klimczuk, R. J. Cava, Rich magnetic phase diagram of the kagome-staircase compound $Mn_3V_3O_8$. *Phys. Rev. B* **76**, 144403 (2007).
9. Y. Chen, J. W. Lynn, Q. Huang, F. M. Woodward, T. Yildirim, G. Lawes, A. P. Ramirez, N. Rogado, R. J. Cava, A. Aharony, O. Entin-Wohlman, A. B. Harris, Complex magnetic order in the kagomé staircase compound $Co_3V_2O_8$. *Phys. Rev. B* **74**, 014430 (2006).
10. N. R. Wilson, O. A. Petrenko, G. Balakrishnan, Magnetic phase diagrams of the kagomé staircase compounds $Co_3V_2O_8$ and $Ni_3V_2O_8$. *J. Phys. Condens. Matter* **19**, 145257 (2007).
11. Y. Yasui, Y. Kobayashi, M. Soda, T. Moyoshi, M. Sato, N. Igawa, K. Kakurai, Successive magnetic transitions of the kagomé staircase compound $Co_3V_2O_8$ studied in various magnetic fields. *J. Phys. Soc. Jpn.* **76**, 034706 (2007).

12. F. Yen, R. P. Chaudhury, E. Galstyan, B. Lorenz, Y. Q. Wang, Y. Y. Sun, C. W. Chu, Magnetic phase diagrams of the kagomé staircase compound $Co_3V_2O_8$. *Physica B Condens. Matter* **403**, 1487–1489 (2008).
13. J. S. Helton, Y. Chen, G. L. Bychkov, S. N. Barilo, N. Rogado, R. J. Cava, J. W. Lynn, Evolution of the commensurate and incommensurate magnetic phases of the *S*=3/2 kagome staircase $Co_3V_2O_8$ in an applied field. *J. Phys. Condens. Matter* **24**, 016003 (2012).
14. X. Zhao, J. C. Wu, Z. Y. Zhao, Z. Z. He, J. D. Song, J. Y. Zhao, X. G. Liu, X. F. Sun, X. G. Li, Heat switch effect in an antiferromagnetic insulator $Co_3V_2O_8$. *Appl. Phys. Lett.* **108**, 242405 (2016).
15. M. Kenzelmann, A. B. Harris, A. Aharony, O. Entin-Wohlman, T. Yildirim, Q. Huang, S. Park, G. Lawes, C. Broholm, N. Rogado, R. J. Cava, K. H. Kim, G. Jorge, A. P. Ramirez, Field dependence of magnetic ordering in kagomé-staircase compound $Ni_3V_2O_8$. *Phys. Rev. B* **74**, 014429 (2006).
16. G. Ehlers, A. A. Podlesnyak, S. E. Hahn, R. S. Fishman, O. Zaharko, M. Frontzek, M. Kenzelmann, A. V. Pushkarev, S. V. Shiryaev, S. Barilo, Incommensurability and spin dynamics in the low-temperature phases of $Ni_3V_2O_8$. *Phys. Rev. B* **87**, 214418 (2013).
17. G. Lawes, A. B. Harris, T. Kimura, N. Rogado, R. J. Cava, A. Aharony, O. Entin-Wohlman, T. Yildirim, M. Kenzelman, C. Broholm, A. P. Ramirez, Magnetically driven ferroelectric order in $Ni_3V_2O_8$. *Phys. Rev. Lett.* **95**, 087205 (2005).
18. I. Cabrera, M. Kenzelmann, G. Lawes, Y. Chen, W. C. Chen, R. Erwin, T. R. Gentile, J. B. Leão, J. W. Lynn, N. Rogado, R. J. Cava, C. Broholm, Coupled magnetic and ferroelectric domains in multiferroic $Ni_3V_2O_8$. *Phys. Rev. Lett.* **103**, 087201 (2009).
19. F. Fabrizi, H. C. Walker, L. Paolasini, F. de Bergevin, T. Fennell, N. Rogado, R. J. Cava, T. Wolf, M. Kenzelmann, D. F. McMorrow, Electric field control of multiferroic domains in $Ni_3V_2O_8$ imaged by x-ray polarization-enhanced tomography. *Phys. Rev. B* **82**, 024434 (2010).
20. L. I. Vergara, J. Cao, L.-C. Tung, N. Rogado, F. Yen, Y. Q. Wang, R. J. Cava, B. Lorenz, Y.-J. Wang, J. L. Musfeldt, Magnetoelastic coupling in magnetically frustrated $Co_3V_2O_8$. *Phys. Rev. B* **81**, 012403 (2010).
21. N. Bellido, C. Martin, C. Simon, A. Maignan, Coupled negative magnetocapacitance and magnetic susceptibility in a kagomé staircase-like compound $Co_3V_2O_8$. *J. Phys. Condens. Matter* **19**, 056001 (2007).
22. M. Ramazanoglu, C. P. Adams, J. P. Clancy, A. J. Berlinsky, Z. Yamani, R. Szymczak, H. Szymczak, J. Fink-Finowicki, B. D. Gaulin, Spin waves in the ferromagnetic ground state of the kagome staircase system $Co_3V_2O_8$. *Phys. Rev. B* **79**, 024417 (2009).
23. S. Toth, B. Lake, Linear spin wave theory for single-Q incommensurate magnetic structures. *J. Phys. Condens. Matter* **27**, 166002 (2015).
24. N. Qureshi, M. Zbiri, J. Rodríguez-Carvajal, A. Stunault, E. Ressouche, T. C. Hansen, M. T. Fernández-Díaz, M. R. Johnson, H. Fuess, H. Ehrenberg, Y. Sakurai, M. Itou, B. Gillon, T. Wolf, J. A. Rodríguez-Velamazan, J. Sánchez-Montero, Experimental magnetic form factors in $Co_3V_2O_8$: A combined study of *ab initio* calculations, magnetic Compton scattering, and polarized neutron diffraction. *Phys. Rev. B* **79**, 094417 (2009).
25. K. Fritsch, G. Ehlers, K. C. Rule, K. Habicht, M. Ramazanoglu, H. A. Dabkowska, B. D. Gaulin, Quantum phase transitions and decoupling of magnetic sublattices in the quasi-two-dimensional Ising magnet $Co_3V_2O_8$ in a transverse magnetic field. *Phys. Rev. B* **92**, 180404(R) (2015).
26. N. R. Wilson, O. A. Petrenko, G. Balakrishnan, P. Manuel, B. Fåk, Magnetic excitations in the kagomé staircase compounds. *J. Mag. Mag. Mater.* **310**, 1334–1336 (2007).
27. K. Fritsch, Z. Yamani, S. Chang, Y. Qiu, J. R. D. Copley, M. Ramazanoglu, H. A. Dabkowska, B. D. Gaulin, Magnetic order and fluctuations in the presence of quenched disorder in the kagome staircase system $(Co_{1-x}Mg_x)_3 V_2O_8$. *Phys. Rev. B* **86**, 174421 (2012).
28. F. Keffer, Moriya interaction and the problem of the spin arrangements in βMnS. *Phys. Rev.* **126**, 896 (1962).
29. M. Elhajal, B. Canals, C. Lacroix, Symmetry breaking due to Dzyaloshinsky-Moriya interactions in the kagomé lattice. *Phys. Rev. B* **66**, 014422 (2002).
30. M. Pereiro, D. Yudkin, J. Chico, C. Etz, O. Eriksson, A. Bergman, Topological excitations in a kagome magnet. *Nat. Commun.* **5**, 4815 (2014).
31. G. Gitgeatpong, Y. Zhao, P. Piyawongwatthana, Y. Qiu, L. W. Harriger, N. P. Butch, T. J. Sato, K. Matan, Nonreciprocal magnons and symmetry-breaking in the noncentrosymmetric antiferromagnet. *Phys. Rev. Lett.* **119**, 047201 (2017).
32. Y. Onose, T. Ideue, H. Katsura, Y. Shiomi, N. Nagaosa, Y. Tokura, Observation of the magnon Hall effect. *Science* **329**, 297–299 (2010).
33. K. Riedl, D. Guterding, H. O. Jeschke, M. J. P. Gingras, R. Valenti, *Ab initio* determination of spin Hamiltonians with anisotropic exchange interactions: The case of the pyrochlore ferromagnet $Lu_2V_2O_7$. *Phys. Rev. B* **94**, 014410 (2016).
34. I. A. Sergienko, E. Dagotto, Role of the Dzyaloshinskii-Moriya interaction in multiferroic perovskites. *Phys. Rev. B* **73**, 094434 (2006).
35. D. Lebeugle, D. Colson, A. Forget, M. Viret, A. M. Bataille, A. Gukasov, Electric-field-induced spin flop in $BiFeO_3$ single crystals at room temperature. *Phys. Rev. Lett.* **100**, 227602 (2008).
36. M. Brockman, A. Klümper, V. Ohanyan, Exact description of magnetoelectric effect in the spin-$\frac{1}{2}$ XXZ chain with Dzyaloshinskii-Moriya interaction. *Phys. Rev. B* **87**, 054407 (2013).
37. A. A. Mukhin, V. Y. Ivanov, A. M. Kuz'menko, A. Prokhorov, A. A. Pronin, S. N. Barilo, G. L. Bychkov, S. V. Shiryaev, Magnetic and ferroelectric properties of exchange-frustrated multiferroics $(Ni_{1-x}T_x)_3V_2O_8$ (T=Co, Mn, Zn). *JETP Letters* **91**, 147–154 (2010).
38. A. Kumarasiri, G. Lawes, Control of the multiferroic transition in $Ni_3V_2O_8$ by transition metal doping. *Phys. Rev. B* **84**, 064447 (2011).
39. O. A. Petrenko, N. R. Wilson, G. Balakrishnan, D. M. Paul, G. J. McIntyre, Kagome staircase compound $Co_3V_2O_8$ in an applied magnetic field: Single-crystal neutron diffraction study. *Phys. Rev. B* **82**, 104409 (2010).
40. G. Ehlers, A. A. Podlesnyak, M. D. Frontzek, A. V. Pushkarev, S. V. Shiryaev, S. Barilo, Damped spin waves in the intermediate ordered phases in $Ni_3V_2O_8$. *J. Phys. Condens. Matter* **27**, 256003 (2015).

Acknowledgments

Funding: This work was supported by the NIST. **Author contributions:** J.S.H. and J.W.L. conceived the project. S.N.B grew the single-crystal samples. J.S.H., N.P.B., D.M.P., and J.W.L. performed the neutron spectroscopy measurements. J.S.H. performed the data analysis and spin wave modeling. J.S.H. wrote the manuscript with comments from all the other authors. **Competing interests:** The authors declare that they have no competing interests. **Data and materials availability:** The raw data files for these experiments can be accessed at the NIST Center for Neutron Research public FTP site: ftp://ftp.ncnr.nist.gov/pub/ncnrdata/. We have also made the raw data files and parameter files available at https://doi.org/10.18434/M32139. The raw data files can be analyzed using the DAVE software, available at www.ncnr.nist.gov/dave/. The spin wave simulations can be recreated using the SpinW software, available at https://spinw.org/.

Submitted 1 August 2019
Accepted 12 February 2020
Published 1 May 2020
10.1126/sciadv.aay9709

Citation: J. S. Helton, N. P. Butch, D. M. Pajerowski, S. N. Barilo, J. W. Lynn, Three-dimensional magnetism and the Dzyaloshinskii-Moriya interaction in $S = 3/2$ kagome staircase $Co_3V_2O_8$. *Sci. Adv.* **6**, eaay9709 (2020).